Supplementary Information: Hydrogen defects as probes of band alignment in metal-organic frameworks

Khang Hoang*
Center for Computationally Assisted Science and Technology & Department of Physics, North Dakota State University, Fargo, North Dakota 58108, United States

TABLE S1. Structural and electronic properties of PCN-222(2H) and PCN-222(M).

	(2H)	(Mn)	(Fe)	(Ni)	(Cu)	(Zn)	(Pt)
PBE+U (eV)	0	10.0	6.0	6.0	7.0	0	6.0
M at linker		Mn^{2+} $3d^5$	Fe^{2+} $3d^6$	Ni^{2+} $3d^8$	Cu^{2+} $3d^9$	Zn^{2+} $3d^{10}$	Pt^{2+} $5d^8$
Magn. mo. (μ_B)		4.85	3.81	0	0.68	0	0
a, b (Å)	43.40	43.43	43.39	43.31	43.38	43.37	43.38
c (Å)	16.90	16.92	16.92	16.90	16.85	16.92	16.92
M–N (Å)		2.09, 2.11	2.06, 2.07	1.98, 2.00	2.01, 2.03	2.05, 2.06	2.02, 2.03
E_g (eV)	1.72	1.67	1.60	1.90	1.85	1.81	1.98
E_g, expt (eV)	1.75–1.84[a]	1.72–1.86[b]	1.58–2.09[c]	1.88–2.00[d]	1.73–2.03[e]	1.80–1.95[f]	2.05–2.13[g]
E_v (V vs. NHE)	1.41	1.39	1.21	1.46	1.43	1.51	1.66
E_c (V vs. NHE)	−0.31	−0.28	−0.39	−0.45	−0.42	−0.30	−0.32

[a]Refs. [1–7]. [b]Refs. [1, 2]. [c]Refs. [1–3]. [d]Refs. [3, 8]. [e]Refs. [2, 3, 9]. [f]Refs. [1, 2, 6]. [g]Refs. [2, 7].

TABLE S2. Structural and electronic properties of MOF-5, MIL-125, UiO-66, and ZIF-8.

	MOF-5	MIL-125	UiO-66	ZIF-8
HSE(α)	0.05	0.22	0.18	0.20
a, b (Å)	26.12	19.24	20.94	17.04
c (Å)		18.21		
E_g (eV)	3.84	3.55	3.96	5.07
E_g, expt (eV)	3.84–3.88[a]	3.30–3.60[b]	3.78–4.10[c]	4.97[d]
E_v (V, vs. NHE)	2.89	2.69	3.19	3.04
E_c (V, vs. NHE)	−0.96	−0.86	−0.77	−2.04

[a]Refs. [10, 11]. [b]Refs. [12, 13]. [c]Refs. [14–18]. [d]Ref. [19].

[1] T. G. Semerci, A. Melillo, Y. Çimen Mutlu, and H. Garcia, Band alignment of PCN-222 via selection of the metal porphyrin linker for sunlight driven photocatalytic overall water splitting, Catal. Today **423**, 113931 (2023).
[2] Q. Li, K. Wang, H. Wang, M. Zhou, B. Zhou, Y. Li, Q. Li, Q. Wang, H.-M. Shen, and Y. She, Metalloporphyrin-Based Metal–Organic Frameworks for Photocatalytic Carbon Dioxide Reduction: The Influence of Metal Centers, Processes **11**, 1042 (2023).
[3] R. Hariri and S. Dehghanpour, Effective visible-light CO_2 photoreduction over (metallo)porphyrin-based metal–organic frameworks to achieve useful hydrocarbons, Appl. Organomet. Chem. **35**, e6422 (2021).
[4] H.-Q. Xu, J. Hu, D. Wang, Z. Li, Q. Zhang, Y. Luo, S.-H. Yu, and H.-L. Jiang, Visible-Light Photoreduction of CO_2 in a Metal–Organic Framework: Boosting Electron–Hole Separation via Electron Trap States, J. Am. Chem. Soc. **137**, 13440 (2015).

* khang.hoang@ndsu.edu

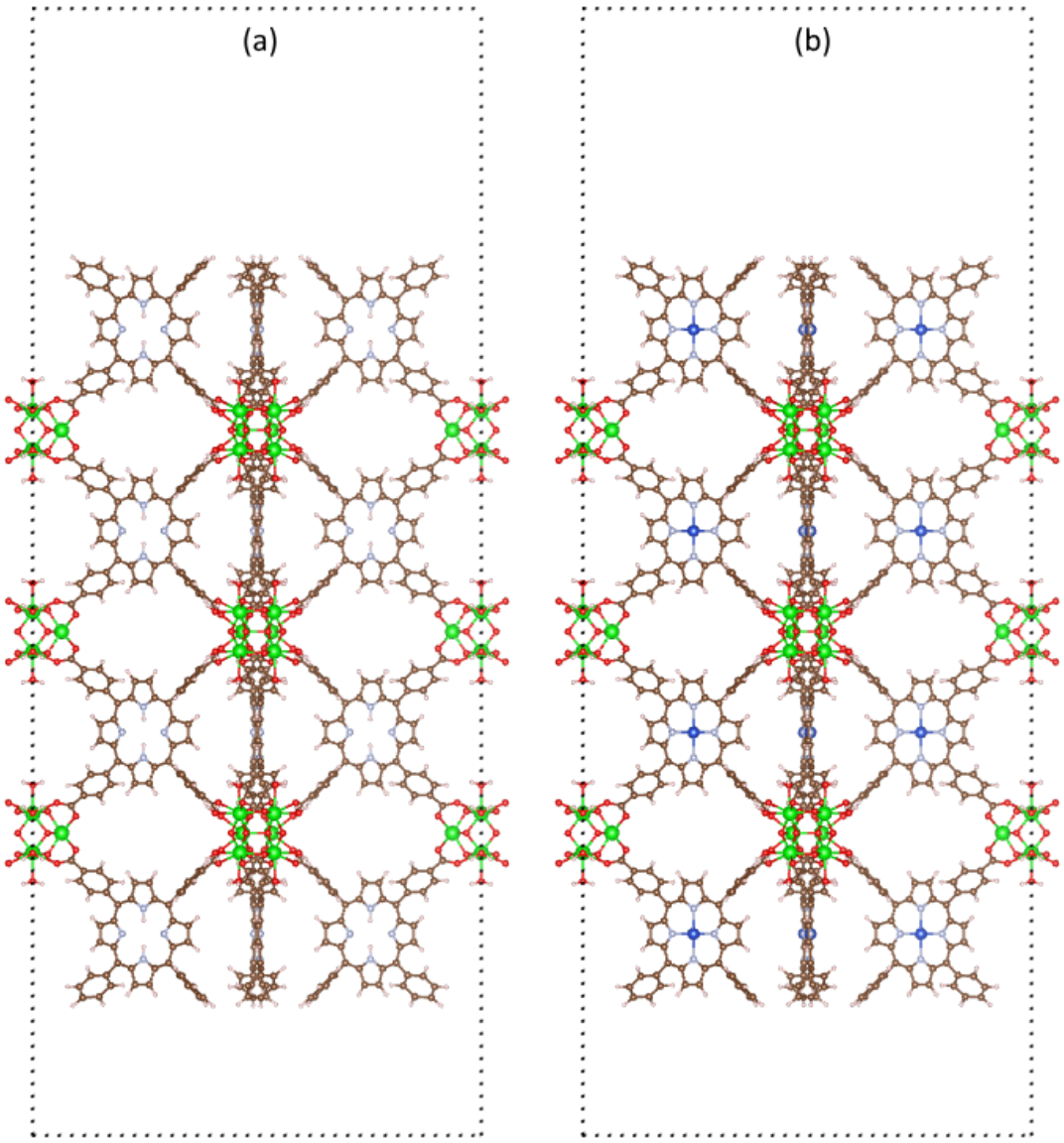

FIG. S1. Slab models for the (001) surface of PCN-222(2H) and PCN-222(Cu). Color code: red = O, brown = C, pink = H, light blue = N, green = Zr, and blue = Cu.

[5] M. Yuan, J. Xue, J. Li, S. Ma, and M. Wang, PCN-222/Ag_2O-Ag p-n heterojunction modified fabric as recyclable photocatalytic platform for boosting bacteria inactivation and organic pollutant degradation, Colloids Surf. A: Physicochem. Eng. Asp. **656**, 130474 (2023).

[6] J. Jin, Porphyrin-based metal–organic framework catalysts for photoreduction of CO_2: understanding the effect of node connectivity and linker metalation on activity, New J. Chem. **44**, 15362 (2020).

[7] H. Zhang, Q. Li, B. Li, B. Weng, Z. Tian, J. Yang, J. Hofkens, F. Lai, and T. Liu, Atomically dispersed Pt sites on porous metal–organic frameworks to enable dual reaction mechanisms for enhanced photocatalytic hydrogen conversion, J. Catal. **407**, 1 (2022).

[8] H. Huang, L. Li, R. Wang, A. R. M. Shaheer, T. Liu, H. Liu, and R. Cao, Assembling phase-junctions based on metal-organic framework polymophism for enhanced overall CO_2 photoreduction activities, Sci. China Mater. **67**, 1839 (2024).

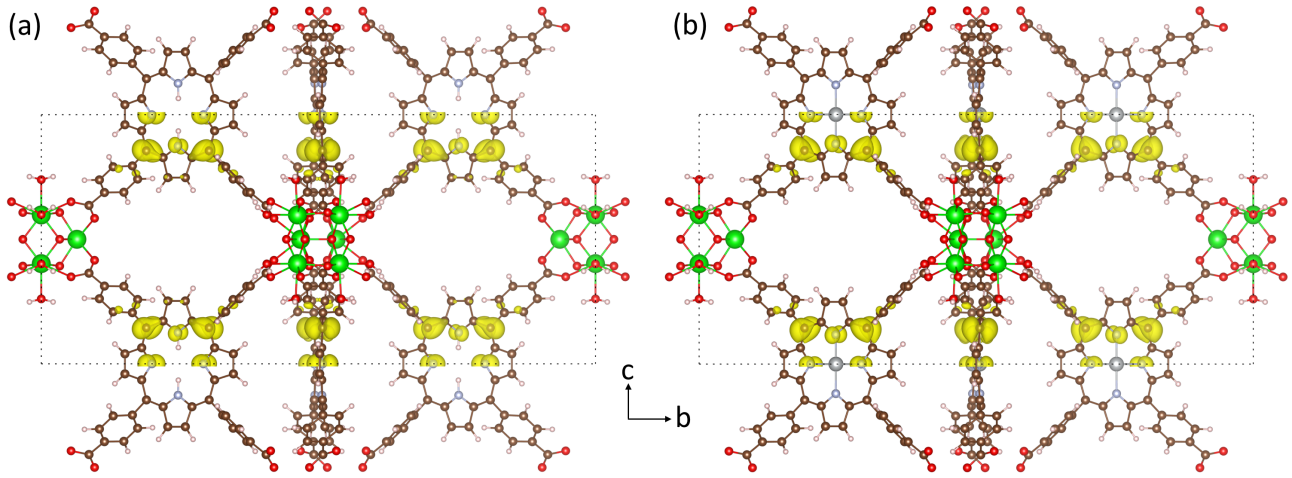

FIG. S2. Structures of (a) PCN-222(2H) and (b) PCN-222(Ni) and charge densities associated with the highest occupied state (VBM). Color code: red = O, brown = C, pink = H, light blue = N, green = Zr, and gray = Ni.

[9] S. Duan, S. Wu, L. Wang, H. She, J. Huang, and Q. Wang, Rod-Shaped Metal Organic Framework Structured PCN-222(Cu)/TiO_2 Composites for Efficient Photocatalytic CO_2 Reduction, Acta Phys. -Chim. Sin. **36**, 1905086. (2020).

[10] T. Yao, Y. Tan, Y. Zhou, Y. Chen, and M. Xiang, Preparation of core-shell MOF-5/Bi_2WO_6 composite for the enhanced photocatalytic degradation of pollutants, J. Solid Stat. Chem. **308**, 122882 (2022).

[11] M. Aleksandrzak, K. Sielicki, and E. Mijowska, Enhancement of photocatalytic hydrogen evolution with catalysts based on carbonized MOF-5 and g-C_3N_4, RSC Adv. **10**, 4032 (2020).

[12] C. Jin, J. Liu, Y. Yin, and Z. Li, WO_3/MIL-125 (Ti) composite material for enhancing the reduction of Cr(VI) under visible light, RSC Adv. **14**, 5142 (2024).

[13] M. Chen, X. Wei, L. Zhao, Y. Huang, S.-C. Lee, W. Ho, and K. Chen, Novel N/Carbon Quantum Dot Modified MIL-125(Ti) Composite for Enhanced Visible-Light Photocatalytic Removal of NO, Ind. Eng. Chem. Res. **59**, 6470 (2020).

[14] X. Mu, J. Jiang, F. Chao, Y. Lou, and J. Chen, Ligand modification of UiO-66 with an unusual visible light photocatalytic behavior for RhB degradation, Dalton Trans. **47**, 1895 (2018).

[15] K. Gayathri, K. Vinothkumar, Y. Teja, B. M. Al-Shehri, M. Selvaraj, M. Sakar, and R. G. Balakrishna, Ligand-mediated band structure engineering and physiochemical properties of UiO-66 (Zr) metal-organic frameworks (MOFs) for solar-driven degradation of dye molecules, Colloids Surf. A: Physicochem. Eng. Asp. **653**, 129992 (2022).

[16] W. Hou, C. Chen, Y. Wang, and Y. Xu, Cerium versus zirconium UiO-66 metal–organic frameworks coupled with CdS for H_2 evolution under visible light, Catal. Sci. Technol. **12**, 4012 (2022).

[17] H.-Q. Xu, S. Yang, X. Ma, J. Huang, and H.-L. Jiang, Unveiling Charge-Separation Dynamics in CdS/Metal–Organic Framework Composites for Enhanced Photocatalysis, ACS Catal. **8**, 11615 (2018).

[18] Y. Sun, T. Huang, W. Feng, G. Zhang, H. Ji, Y. Zhu, H. Zhou, F. Dou, Y. Su, Z. Liu, M. Yang, and H. Pang, Enhanced Photocatalytic Nitrogen Fixation over Nano-UiO-66(Zr) via Natural Chlorophyll Sensitization, Inorg. Chem. **63**, 24876 (2024).

[19] J.-J. Li, Q. Zhang, L.-Y. Zhang, J.-Y. Zhang, Y. Liu, N. Zhang, and Y.-Z. Fang, Interfacial band bending induced charge-transfer regulation over Ag@ZIF-8@g-C_3N_4 to boost photocatalytic CO_2 reduction into syngas, Catal. Sci. Technol. **12**, 3343 (2022).

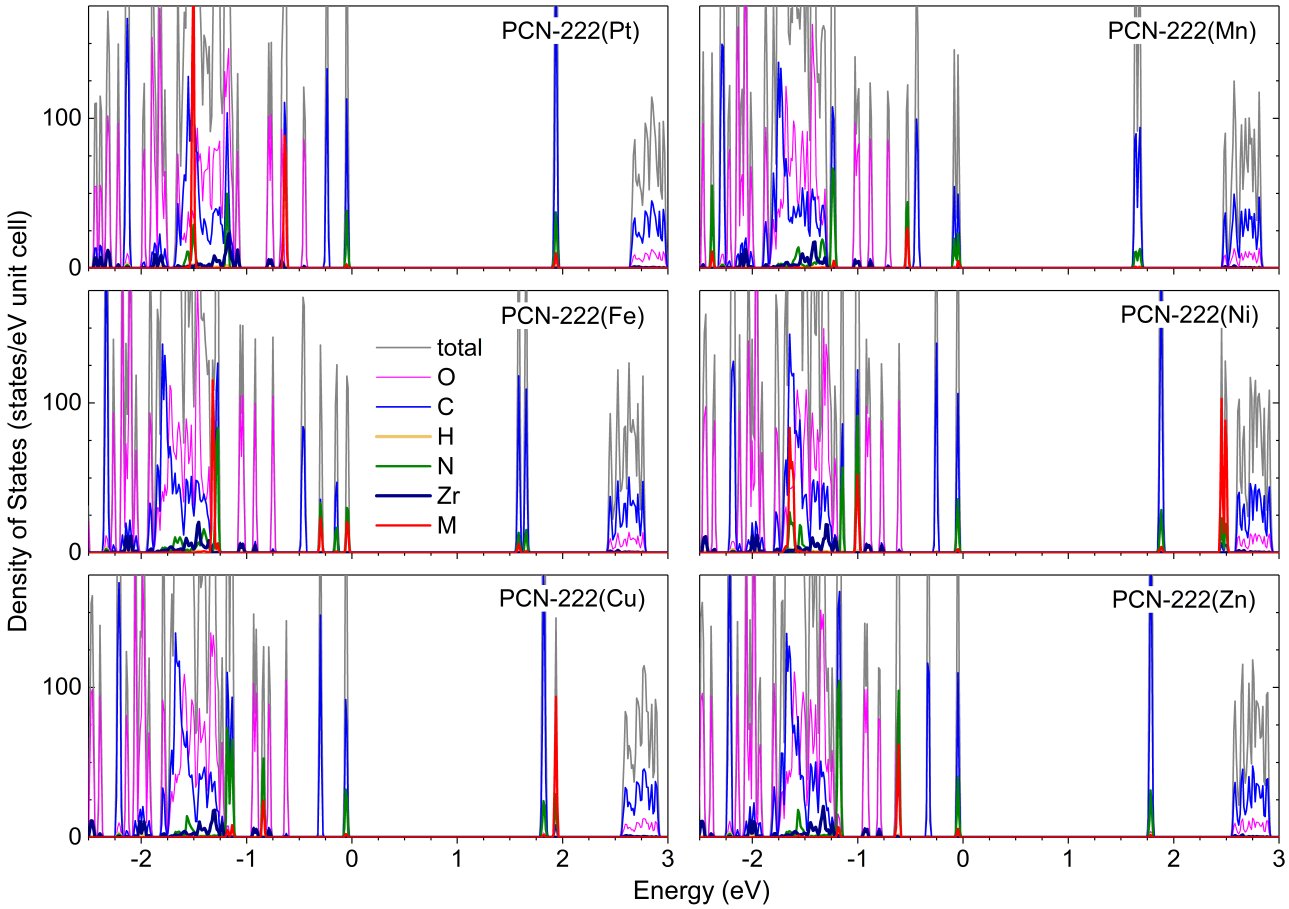

FIG. S3. Total and atom-decomposed electronic densities of states near the band-gap region in PCN-222(M), M = Pt, Mn, Fe, Ni, Cu, and Zn. The zero of energy is set to the highest occupied state.

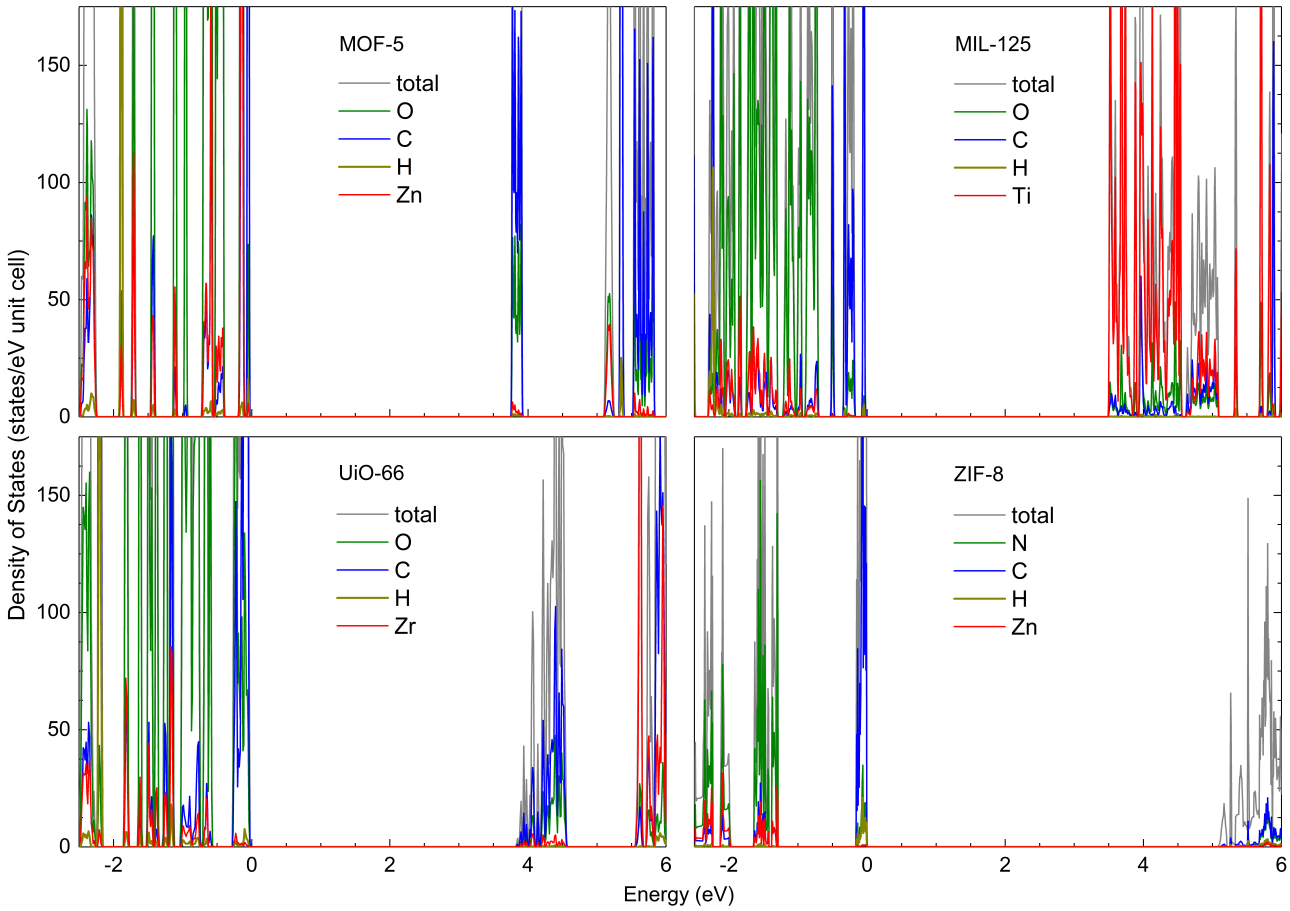

FIG. S4. Total and atom-decomposed electronic densities of states near the band-gap region in MOF-5, MIL-125, UiO-66, and ZIF-8. The zero of energy is set to the highest occupied state.

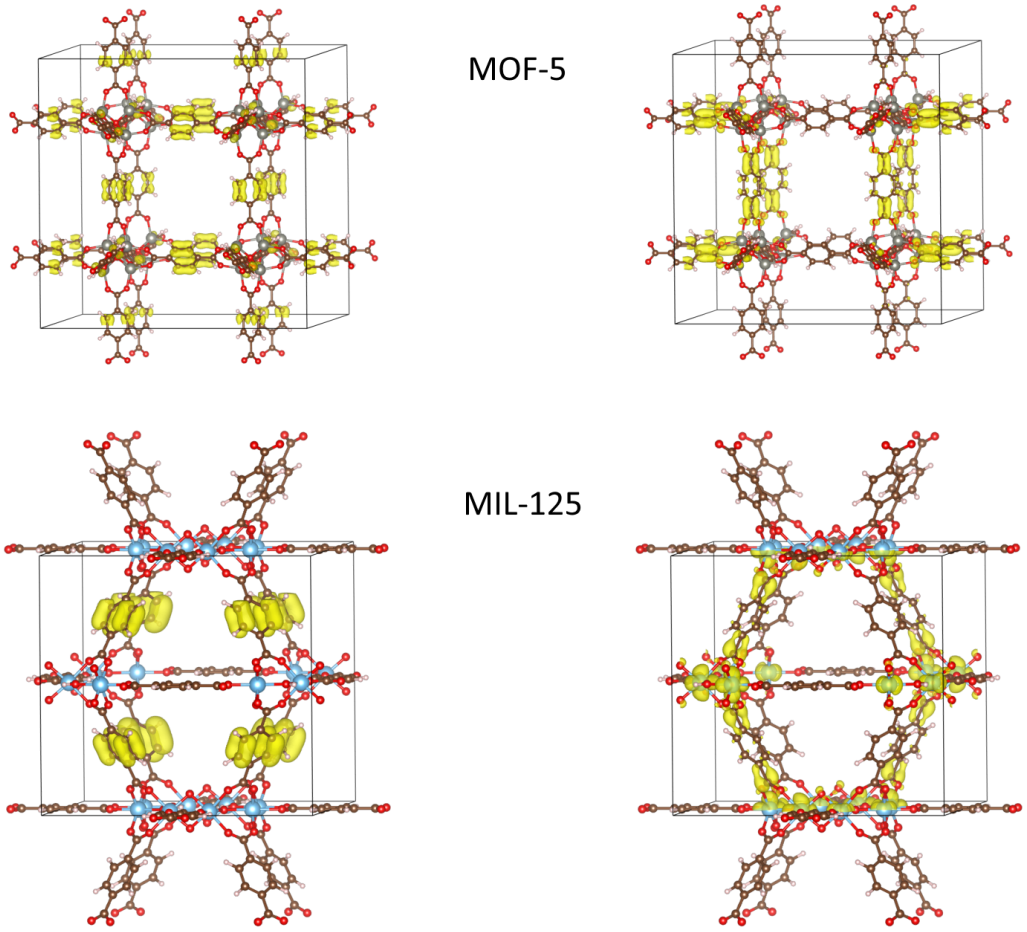

FIG. S5. Structures of MOF-5 and MIL-125 and charge densities associated with the highest occupied state (VBM; left) and the lowest unoccupied state (CBM; right). Color code: red = O, brown = C, pink = H, gray = Zn, and blue = Ti.

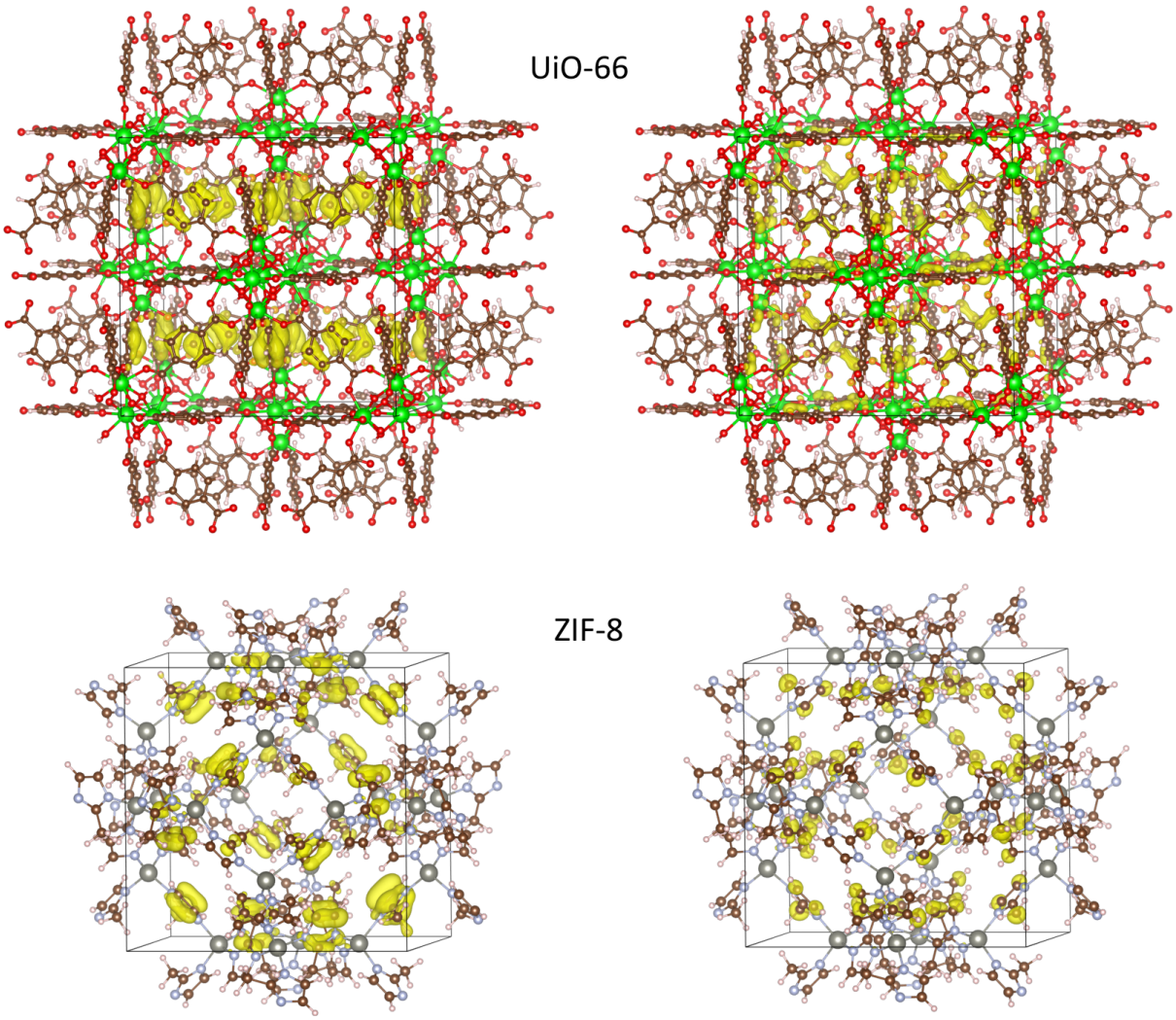

FIG. S6. Structures of UiO-66 and ZIF-8 and charge densities associated with the highest occupied state (VBM; left) and the lowest unoccupied state (CBM; right). Color code: red = O, brown = C, pink = H, green = Zr, and gray = Zn.

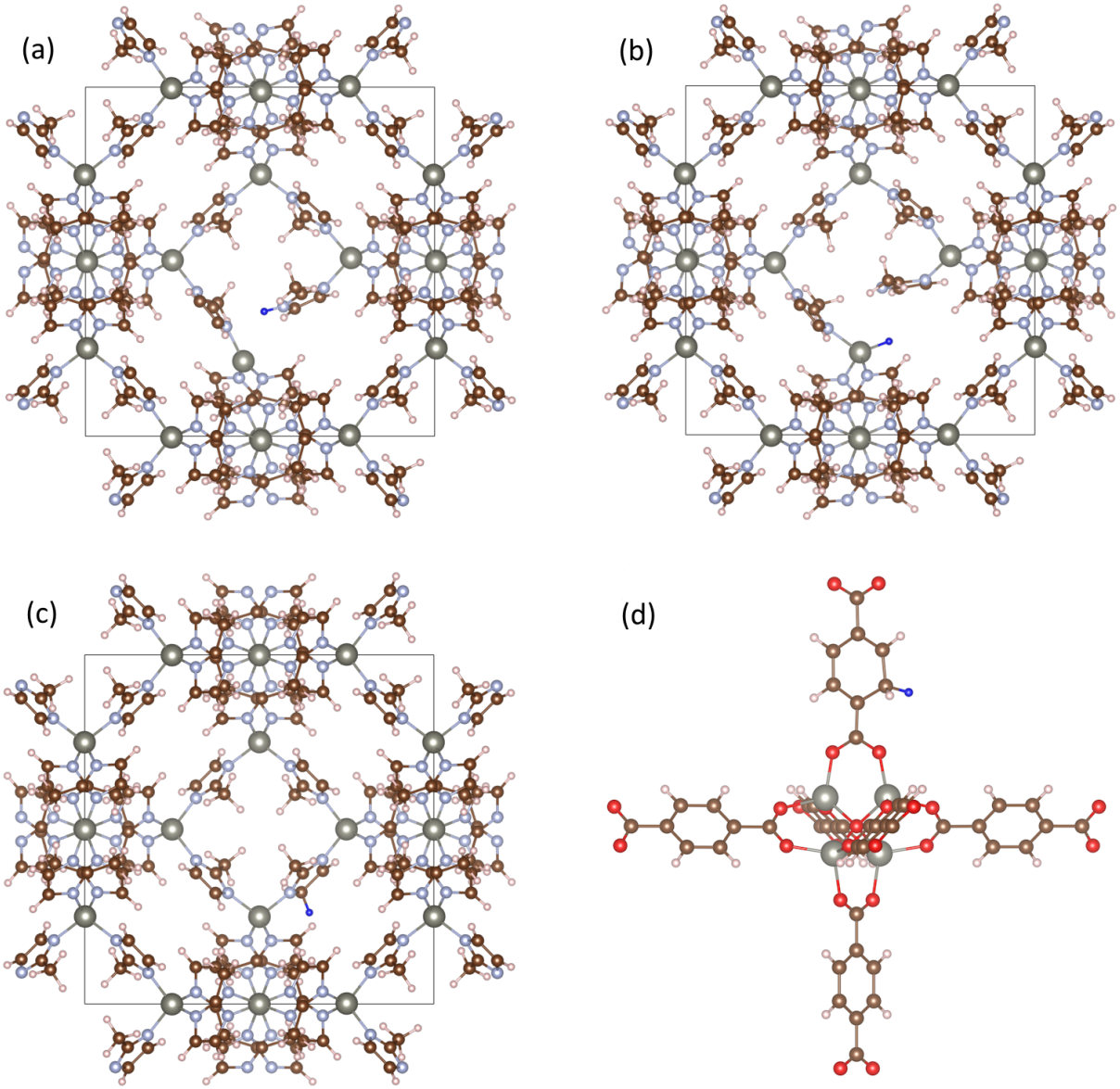

FIG. S7. Local structure of (a) H_i^+ and (b) H_i^- at the SBU and (c) H_i^0 at the 2-mIM linker in ZIF-8, and (d) H_i^- at the BDC linker in MOF-5. H_i is represented by a small blue sphere. Other H_i defects at the BDC linker in MOF-5, MIL-125, and UiO-66 have a similar structure to H_i^- in MOF-5. Color code: red = O, brown = C, pink = H, light blue = N, and gray = Zn.

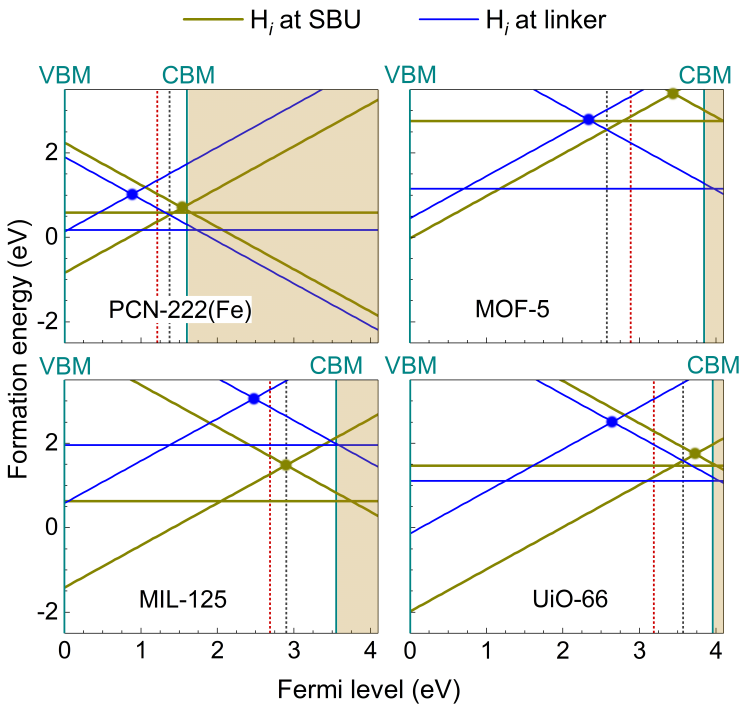

FIG. S8. Formation energies of hydrogen interstitials (H_i), as a function of the Fermi level, in PCN-222(Fe), MOF-5, MIL-125, and UiO-66. H_i^+ (H_i^-) have positive (negative) slopes and horizontal lines correspond to H_i^0. The local $\epsilon(+/-)$ levels of H_i at the SBU and at the linker are marked by large dark yellow and blue solid dots, respectively; the global $(+/-)$ level (determined by the lowest-energy H_i^+ and H_i^-) and the effective $(+/-)$ level (i.e., the average of the local $\epsilon(+/-)$ levels at the SBU and the linker) are marked by the vertical black and red dotted lines, respectively. In this presentation, the hydrogen chemical potential μ_H is set to -0.23 eV [in the case of MOF-5 and UiO-66] or -1.60 eV [PCN-222(Fe) and MIL-125].

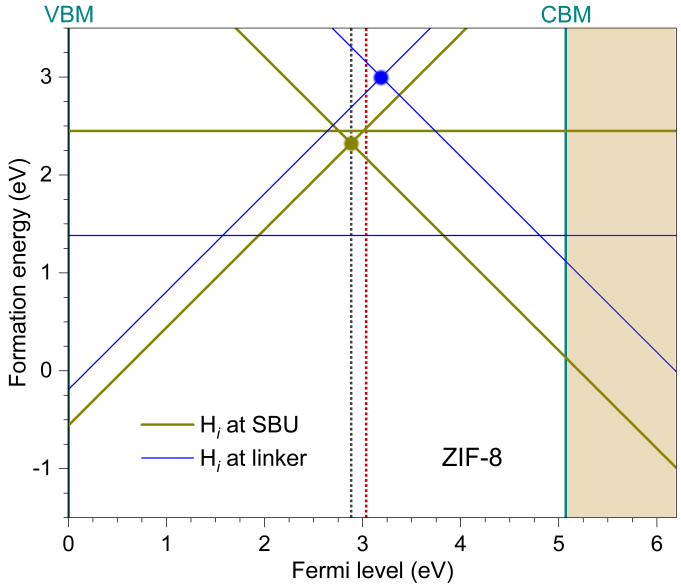

FIG. S9. Formation energies of hydrogen interstitials (H_i) in ZIF-8. The local $\epsilon(+/-)$ levels of H_i at the SBU and at the linker are marked by large solid dark yellow and blue dots, respectively; the global (effective) $(+/-)$ level is marked by the vertical black (red) dotted line. In this presentation, the hydrogen chemical potential μ_H is set to -0.23 eV; see text.